Nuclear Instruments and Methods in Physics Research A 729 (2013) 596–604

Contents lists available at ScienceDirect

Nuclear Instruments and Methods in Physics Research A

journal homepage: www.elsevier.com/locate/nima

Scintillation and detection characteristics of high-sensitivity $CeBr_3$ gamma-ray spectrometers

F.G.A. Quarati [a,b,*], P. Dorenbos [a], J. van der Biezen [c], Alan Owens [c], M. Selle [d], L. Parthier [e], P. Schotanus [f]

[a] Faculty of Applied Science, Department of Radiation Science & Technology, Delft University of Technology, Mekelweg 15, 2629JB Delft, The Netherlands
[b] Praesepe BV, Heilige Geestweg 65, 2201JR Noordwijk, The Netherlands
[c] European Space Agency, ESA/ESTEC, Keplerlaan 1, 2201AZ Noordwijk, The Netherlands
[d] Hellma Materials GmbH, Moritz von Rohrstraße 1, 07745 Jena, Germany
[e] SCHOTT AG, Advanced Materials, Hattenbergstrasse 10, 55122 Mainz, Germany
[f] Scionix Holland BV, Regulierenring 5, 3981LA Bunnik, The Netherlands

ARTICLE INFO

Article history:
Received 10 June 2013
Received in revised form
2 August 2013
Accepted 4 August 2013
Available online 15 August 2013

Keywords:
Cerium-bromide
Lanthanum-bromide
Scintillator gamma-ray spectrometers
Detection sensitivity
Low count rate
Planetary remote sensing

ABSTRACT

Crystal growth and detector fabrication technologies have reached such a state of maturity that high-quality large-volume $CeBr_3$ scintillators can now be produced with dimensions of $2'' \times 2''$ and well above. We present a study of $CeBr_3$ samples of various dimensions and show that they have a number of advantages over equivalently sized $LaBr_3$:5%Ce for gamma-ray spectroscopy applications requiring high detection sensitivity.

At the present time, the achieved energy resolution of $CeBr_3$ is about 4% FWHM at 662 keV, i.e. 25% worse than that of $LaBr_3$:5%Ce. However, thanks to the drastically reduced intrinsic activity, $CeBr_3$ gamma-ray detection sensitivity is about 1 order of magnitude better than that of $LaBr_3$:5%Ce at energies of 1461 keV and 2614.5 keV, which are relevant for the detection of ^{40}K and ^{208}Tl (^{232}Th), respectively.

In this communication, we report on several aspects of $CeBr_3$ gamma-ray spectrometers, such as scintillation characteristics, non-proportionality of the response, gamma-ray detection performances up to 3 MeV and radiation tolerance.

1. Introduction

For many gamma-ray spectroscopy applications a common problem is dealing with low intensity gamma-ray emissions. This is particularly true for remote gamma-ray spectroscopy of planetary surfaces where the gamma-ray flux is very low. For example, for Mars and Mercury, it is of the order of few counts per minute per cm^2 [1,2]. Similarly, for homeland security applications, the successful detection of illegal nuclear material must rely on high detection sensitivity. In fact inspections must last as short as reasonably possible while attempting to mitigate for the illegal-trader's counter-measures.

The new lanthanide scintillators are particularly attractive for the above applications, bridging the gap between the simple-to-use but relatively low-energy-resolution conventional scintillators (e.g. NaI(Tl)) and the more complex high-energy-resolution cryogenically-cooled semiconductor detectors (e.g. HPGe). A $LaBr_3$:5%Ce is in fact the choice for the gamma-ray spectrometer onboard BepiColombo ESA/JAXA mission to Mercury [3].

However, the intrinsic presence of ^{138}La poses limits to $LaBr_3$:5%Ce wider applications [4]. The decays of such a naturally occurring radioactive isotope partially spoil its detection performance, particularly for energies below 1.5 MeV. As investigated in the present study, the recently available $CeBr_3$ is an optimum compromise between an ideal ^{138}La-free- $LaBr_3$:5%Ce and $LaBr_3$:5%Ce itself, offering concrete advantage over $LaBr_3$:5%Ce for the detection of low intensity gamma rays.

Our research on $CeBr_3$ for space applications started in 2006 in parallel with the development of large $LaBr_3$:5%Ce crystals for the BepiColombo mission to Mercury [5]. However, it is only in early 2012 that $CeBr_3$ gamma-ray spectrometers as large as large $2'' \times 2''$ (Fig. 1) were developed by SCHOTT AG and Scionix Holland BV, where Hellma Materials GmbH has taken over the activities of SCHOTT AG [6–8]. At the present time, $CeBr_3$ crystals are routinely grown as $3¼''$ boules by Hellma Materials GmbH and high-quality $3'' \times 4''$ scintillators detectors have been already fabricated by Scionix Holland BV with energy resolution unaffected by their larger size.

This article is organized as follows. In Section 2 we give a description of the samples used and then, in Section 3, we report

* Corresponding author at: Faculty of Applied Science, Department of Radiation Science & Technology, Delft University of Technology, Mekelweg 15, 2629JB Delft, The Netherlands. Tel.: +31 0 15 278 1398; fax: +31 0 15 278 8303.
E-mail address: F.G.A.Quarati@tudelft.nl (F.G.A. Quarati).

0168-9002/$ - see front matter © 2013 Elsevier B.V. All rights reserved.
http://dx.doi.org/10.1016/j.nima.2013.08.005

Fig. 1. Picture of two of the $CeBr_3$ encapsulated samples used in this study, left $1'' \times 1''$ sample SFC 273 (proton irradiated) and right $2'' \times 2''$ sample SBF 307.

on the experimental characterization of $CeBr_3$ scintillation and correlate the results with the characteristic Ce^{3+} scintillation mechanism proper also of $LaBr_3$:5%Ce. Section 4 is dedicated to the energy resolution response (up to 3 MeV) of $2'' \times 2''$ $CeBr_3$ with a comparison with equivalently sized $LaBr_3$:5%Ce. Section 5 reports on $CeBr_3$ intrinsic activity. Section 6 summarizes the result of Section 4 and Section 5 in terms of spectrometer sensitivity. In Section 7, we briefly report on $CeBr_3$ proton irradiation and radiation tolerance assessment and in Section 8 we summarize and conclude.

2. Samples description

$CeBr_3$, like other scintillators and in particular $LaBr_3$:5%Ce, is highly hygroscopic and samples must be handled carefully to avoid any contact with air and/or moisture. The samples used are reported in the first column of Table 1 that includes encapsulated and bare samples. Bare samples have been handled inside a nitrogen filled glove box to prevent any hydration and, to carry out measurements outside the glove box, mounted inside customized hermetic enclosures. The encapsulated samples are sealed in aluminum containers provided with quartz window for scintillation light readout (see Fig. 1). Because the applications of $CeBr_3$ as gamma-ray spectrometers is our main interest, the study mostly focuses on $2'' \times 2''$ $CeBr_3$, being the largest and most detection efficient encapsulated samples we had available. Smaller bare samples have been used primarily for scintillation characterization like scintillation emission spectrum and decay time measurements.

For comparative studies, a standard $2'' \times 2''$ $LaBr_3$:5%Ce (Brillance380 by Saint Gobain [9]) and a standard $2'' \times 2''$ NaI(Tl) were also used. The actual $2'' \times 2''$ $LaBr_3$:5%Ce is the same used in a previous study [10] from which we took the data on energy resolution used in the present study. In addition, [10] together with [11] provide detailed background information for properly operating $LaBr_3$:5%Ce crystals coupled with photomultiplier tubes (PMTs) and, as described in the next sections, being $CeBr_3$ scintillation characteristics very similar to that of $LaBr_3$:5%Ce, the techniques developed for the latter are directly applicable to the first, above all the careful setting of PMT bias, and/or its voltage divider, in order to avoid any signal saturation.

3. $CeBr_3$: material and scintillation characteristic

$LaBr_3$:5%Ce is a solid solution of 95% $LaBr_3$ and 5% $CeBr_3$. Both $LaBr_3$ and $CeBr_3$ crystals have the uranium tri-chloride (UCl_3) lattice type with an asymmetrical hexagonal crystal structure (screw axis) and a non-isotropic thermal expansion coefficient which induces a propensity to crack during the cooling down following the crystal growth.

Table 1
Summary of light yield (LY) and energy resolution measurements with bare and encapsulated $CeBr_3$ crystals. The measurement systematic error for the yields is $\pm 10\%$ relative to the value and for the energy resolutions is $\pm 0.15\%$ absolute.

Sample	Photo-electron yield (phe/MeV)	Absolute light yield (photon/MeV)	Energy resolution at 662 keV %
$CeBr_3$ bare samples			
#4 (2 mm thick)	17,000	59,000	4.1
#5 (3 mm thick)	17,500	60,000	4.2
#6 (3 mm thick)	19,000	66,000	3.7
DU001 ($0.5'' \times 1''$)	16,500	57,000	4.3
Bare sample average	17,500	60,000	4.1
$CeBr_3$ encapsulated samples			
SBG 388 ($1'' \times ⅛''$)	13,000	45,000	4.2
SFC 269 ($1'' \times 1''$)	11,500	40,000	4.4
SFC 270 ($1'' \times 1''$)	12,500	43,000	4.2
SFC 271 ($1'' \times 1''$)	13,000	45,000	4.4
SFC 272 ($1'' \times 1''$)	13,500	47,000	4.7
SFC 273 ($1'' \times 1''$)	13,500	47,000	4.5
SBX 431 ($2'' \times 2''$)	12,500	43,000	4.3
SFB 307 ($2'' \times 2''$)	12,500	43,000	4.2
SFB 308 ($2'' \times 2''$)	12,500	43,000	4.1
Encapsulated sample average	13,000	45,000	4.3
$LaBr_3$:5%Ce encapsulated sample			
Typical	19,000	66,000	3.1

Compared to La, Ce ionic radius is smaller, 122 pm vs. 120 pm [12], and $CeBr_3$ effective atomic number Z_{eff} is larger than that of $LaBr_3$:5%Ce, 45.9 vs. 45.3, respectively. As a consequences, $CeBr_3$ density is slightly larger than that of $LaBr_3$:5%Ce, 5.18 g/cm^3 vs. 5.07 g/cm^3. Given the slightly larger Z_{eff} of $CeBr_3$, a few per cent advantage in detection efficiency compared to $LaBr_3$:5%Ce is expected for $CeBr_3$ at energies dominated by pair production where the interaction probability rises approximately as Z_{eff}^2.

3.1. Emission spectrum and self-absorption

$CeBr_3$ is characterized by a similar Ce^{3+} scintillation mechanism as in $LaBr_3$:5%Ce [5,13]. The Ce^{3+} emission is always due to the transition from the lowest 5d level to the spin orbit split 4f ground state leading to the characteristic double emission band observed clearly in Fig. 2. The emission of our recently developed $CeBr_3$ crystals peaks at 370 nm as compared to 360 nm of $LaBr_3$:5%Ce already reported by [13] and not at 390 nm as reported for earlier available material [5]. Fig. 2 shows the X-ray excited emission of three $CeBr_3$ samples of equivalent quality, with variable thicknesses of ~0.25 mm, ~2.5 mm and ~25 mm (~1″). The X-rays were oriented on the sample's side opposite to the entrance window of the monochromator. Results are that each sample is characterized by a slightly different emission spectrum, shifting towards longer wavelength with increased sample thickness. In parallel, the relative intensity of the two emission peaks tends to equalize. These effects are due to scintillation self-absorption and re-emission processes [5,14] as described in the following paragraphs.

Depending on the actual Ce^{3+} concentration, the short wavelength side of the Ce^{3+} emission can be absorbed by other Ce^{3+} ions and re-emitted as a double band emission. In other words the short wavelength part is re-distributed over the entire double band spectrum. When this is repeated several times the net effect is a shift and a narrowing of the emission profile. $LaBr_3$:5%Ce

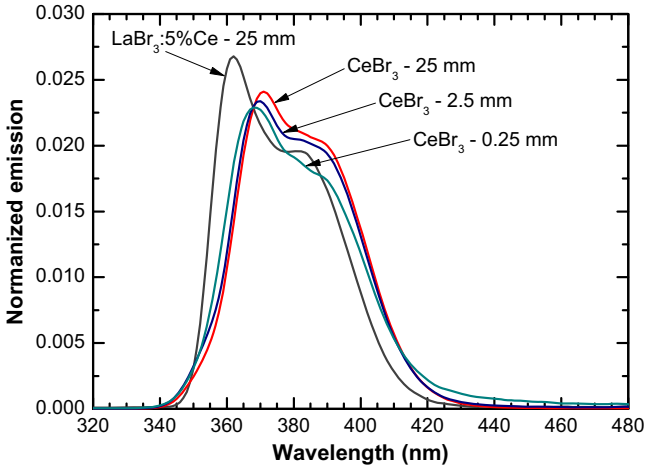

Fig. 2. X-ray excited emission of $CeBr_3$ and $LaBr_3$:5%Ce. For $CeBr_3$, the emission of three samples with increasing thicknesses is presented. The spectra are area normalized.

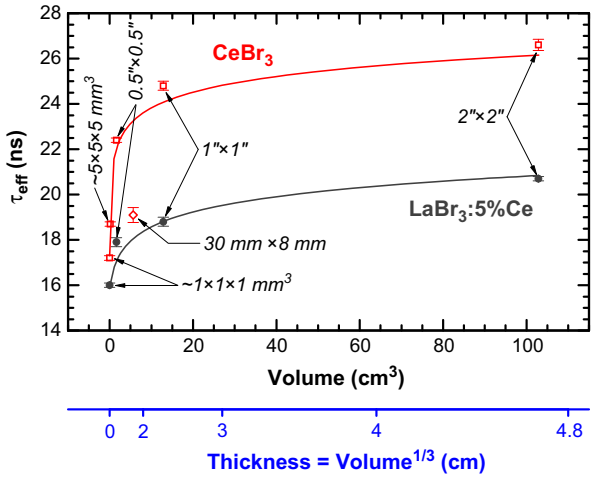

Fig. 3. Scintillation decay time under ^{137}Cs excitation for both $CeBr_3$ and $LaBr_3$:5% Ce samples of several volumes. The two lines are interpolating logarithmic functions to guide the eyes. The 30 mm × 8 mm $CeBr_3$ sample represents a deviant data point (open diamond data symbol) which is attributed to its particular aspect ratio.

contains 20 times less Ce^{3+} than $CeBr_3$ and based on that, in the first approximation, one expects that a 20 times smaller $CeBr_3$ sample would show the same emission spectrum of $LaBr_3$:5%Ce. In Fig. 2, we see that this is not the case and even a 100 times smaller $CeBr_3$ still presents a shifted emission. We assume that the emission of the smaller available $CeBr_3$ sample (0.25 mm) is very close to the $CeBr_3$ intrinsic emission. Apparently its smaller lattice parameter and site size causes an intrinsic ~5 nm blue-shift of the Ce^{3+} emission in $CeBr_3$ as compared to $LaBr_3$:5%Ce. Such a shift does not have any influence on the collection efficiency when the crystal is coupled to a PMT with bialkali photocathode.

3.2. Scintillation decay time

Scintillation decay time measurements were carried out with a set of $CeBr_3$ and $LaBr_3$:5%Ce samples using a technique based on [15], using ^{137}Cs as excitation source and uniformly irradiating the sample along its axis. For both materials, the samples were characterized by an increasing size ranging from $\sim 1\times 1\times 1$ mm^3 up to $2''\times 2''$ (102.9 cm^3). The measured $1/e$ decay time constants (τ_{eff}) for all samples are plotted in Fig. 3 together with interpolating logarithmic functions to guide the eyes.

For both $CeBr_3$ and $LaBr_3$:5%Ce, the Ce^{3+} emission is characterized by a short radiative life time resulting in an intrinsic $1/e$ decay time constant, τ, of 17 ns and 15 ns, respectively [5,16]. As seen in Fig. 3 the smallest available $CeBr_3$ and $LaBr_3$:5%Ce samples ($\sim 1\times 1\times 1$ mm^3) both indeed show decay time constants in agreement with that values, 17.2 ns and 16.0 ns respectively.

However, we found that for both materials τ_{eff} increases with sample size, as shown in Fig. 3, up to 26.6 ns for $CeBr_3$ and 20.7 ns for $LaBr_3$:5%Ce. Beside smaller contributions due to light transport inside the crystal (~1 ns), such an increase is again attributed to scintillation self-absorption and re-emission mechanism which occurs to a lesser extent in $LaBr_3$:5%Ce as well. We can again apply the idea that a $LaBr_3$:5%Ce sample 20 times larger than a $CeBr_3$ sample presents similar behavior to the latter because of their equal absolute Ce concentration. We measured τ_{eff} of 20.7 ns with the $2''\times 2''$ $LaBr_3$:5%Ce (102.9 cm^3) and, by linear interpolation of the $0.5''\times 0.5''$ and $1''\times 1''$ data points in Fig. 3, we could evaluate τ_{eff} ~23 ns with an hypothetical 5 cm^3 $CeBr_3$ sample, in reasonable agreement.

At every absorption and re-emission cycle, the direction of the absorbed photon is lost since the new photon is re-emitted isotropically. If the mean free path of a photon is much smaller than the crystal dimension, the photon will change direction many times before being reflected by the reflective tape at the crystal edge and/or eventually be absorbed at the PMT photocathode. Using τ_{eff} we can evaluate the average number of emission–absorption–emission cycles occurred before a photon escapes the crystal to be collected by:

$$\tau_{\mathrm{eff}} = \tau/\beta \tag{1}$$

where β is the probability that an emitted photon escapes the scintillator without having been re-absorbed along its entire travel path. Eq. (1) gives an excellent tool to determine β simply using the measured τ_{eff}. For a $2''\times 2''$ $CeBr_3$, τ_{eff}=26.6 ns so then β=0.64, meaning that on average 64% of the scintillation photon escape the crystal without the occurrence of an absorption and re-emission cycle. In case of $LaBr_3$:5%Ce the probability is 72%.

Since real crystals are always characterized by presence of impurities that may absorb photons, the capability of the scintillation light to quickly escape the crystal to be collected at the PMT photocathode is an important aspect for the preservation of the light yield and therefore of the energy resolution. The longer the distance a photon has to travel inside the crystal the higher is the probability to be lost. In addition, when many cycles occur, the number of cycles strongly depends on the point of interaction which may cause inhomogeneous performance and degrade the energy resolution.

3.3. Scintillation light yield

Scintillation light yield (LY) measurements were based on the method described in [17,18]. It consists of measuring the mean value of the signal corresponding to the detection of a single photoelectron (sphe) and using it to normalize the peak position corresponding to the detection of a given gamma-ray energy −662 keV (^{137}Cs) in our case. If the quantum efficiency of the PMT is known at the scintillation emission wavelengths, the absolute scintillation light yield can also be evaluated. Our LY evaluation does not include correction for the photocathode reflectivity.

In order to maximize scintillation light collection, all measurements were carried out using optical grease between crystal and PMT and spanning several layers of reflective PTFE tape over the crystal and PMT, i.e. the umbrella configuration in [18]. The PMT for these measurements was a 2″ Hamamatsu R1791 (Quartz window version of R878) for which the signal was extracted from

the 6th dynode, in order to avoid signal saturation [11,19]. Averaged over the scintillation emission spectrum of $CeBr_3$ or $LaBr_3$:5%Ce, the quantum efficiency of the particular PMT we used is 29% in both cases.

Results of LY measurement are reported in Table 1. For comparison, consistent data corresponding to the typical performance of an encapsulated $LaBr_3$:5%Ce are also reported. On average, $CeBr_3$ bare samples show higher light yield compared to encapsulated samples, however without a corresponding improvement in the energy resolution, apparently indicating that contributions other that Poisson statistics are also present. The LY of $CeBr_3$ is also affected by self-absorption and re-emission processes, and the corresponding larger probability of photon loss which makes the average LY of $CeBr_3$ encapsulated samples 68% of that typically achievable with $LaBr_3$:5%Ce.

3.4. Scintillation non-proportionality of the response (nPR)

Scintillators typically show a non-proportionality of the response which affects their energy resolution (nPR) [4,20]. An efficient technique to characterize such a behavior is the use of monochromatic synchrotron radiation [21,22]. Fig. 4 shows the measured nPR of $CeBr_3$ and $LaBr_3$:5%Ce. The $LaBr_3$:5%Ce data are taken from [21] and normalized to unity at 100 keV. $CeBr_3$ data are from this work and collected using crystal SBG 388 (Table 1). $CeBr_3$ and $LaBr_3$:5%Ce nPR curves normalized at 662 keV are available in [22], collected with different samples.

A possible way to characterize the nPR is by the area between the actual nPR curve and the ideal nPR as indicated in Fig. 4 [20]. Such an area for $CeBr_3$ is about 1.65 times larger than the corresponding area for $LaBr_3$:5%Ce. The brighter among $CeBr_3$ bare samples (#6 in Table 1) matches the LY of encapsulated $LaBr_3$:5%Ce but not the energy resolution, consistently with the observed nPR characteristics.

The processes at the origin of the nPR are extremely complex and today the level of knowledge is not sufficient to provide a comprehensive description of the phenomenon which has, however, been widely and deeply addressed, see e.g. [23–25]. An attempt to explain nPR is as follows. At the start of the scintillation process is the charge transport efficiency to the luminescence centers. This appears to also depend on the ionization density created in the crystal by an X- or gamma-ray interaction, which, in turn, increases with lower energy of the electrons originating from the interaction. The increasing of the ionization density would then also increase the occurrence of phenomena in competition with the scintillation process, as non-radiative recombinations, making the charge transport to the luminescence center less efficient. This would lead to a scintillation yield that is no longer proportional to the number of ionization created or, equivalently, to the energy of the detected X- or gamma ray. The scintillator energy resolution is ultimately affected because of the stochastic repartition of the primary X- or gamma ray energy among the excited electrons [4].

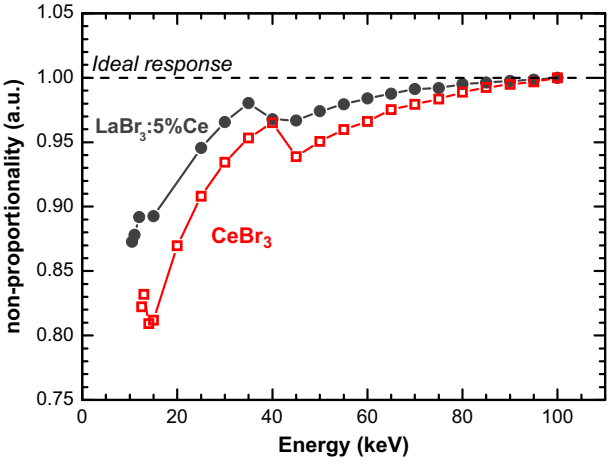

Fig. 4. Synchrotron measurements of the non-proportionality of the response (nPR) of $CeBr_3$ and $LaBr_3$:5%Ce. The curves are normalized to 1 at 100 keV.

Alpha particle interactions may create much higher ionization density than electron (or X- or gamma-ray) interactions and, applying the previous interpretation of the nPR, alpha particle interactions would then be characterized by a further reduced charge transport efficiency. We can then presume that the so called alpha/gamma scintillation ratio, i.e. the lower light yield generated by alpha particles compared to gamma rays (or electrons) of equivalent energy, originates from the same deterioration of the charge transport efficiency responsible for the nPR. As it will be presented in Section 5, the alpha/gamma scintillation ratio we observed with $CeBr_3$ is indeed sensibly lower than that observed with $LaBr_3$:5%Ce. This would mean that in $CeBr_3$ the charge transport efficiency is more strongly affected than in $LaBr_3$:5%Ce by the higher ionization density, in this case of the alpha particles, again consistently with the observed nPR characteristics.

4. X- and gamma-ray energy resolution

In order to collect gamma-ray pulse height spectra with radioactive sources and investigate the energy resolution as a function of energy, we used for the $2'' \times 2''$ $CeBr_3$ the setup already optimized for $LaBr_3$:5%Ce [10]. The set up is based on a 2″ R6231 Hamamatsu PMT with a cathode blue sensitivity of ~13 μA/LmF (~30% QE) and operated at +520 V.

In Figs. 5 and 6 pulse height spectra of ^{137}Cs and ^{152}Eu are shown, collected with the $2'' \times 2''$ $CeBr_3$ "SFB 308" of Table 1, the $2'' \times 2''$ $LaBr_3$:5%Ce of [10] and, for further reference, with the $2'' \times 2''$ NaI(Tl). All the spectra are from this work and normalized by the acquisition time and by the keV per channel. For all spectrometers, the same setup has been used and the same source position, 25 cm above the crystal top face. The energy resolutions FWHM at 662 keV achieved by the three spectrometers are: 21.1 keV for $LaBr_3$:5%Ce, 27.2 keV $CeBr_3$ and 47.3 keV for NaI(Tl), i.e. 3.2%, 4.1% and 7.2%. The 3.2% energy resolution of $LaBr_3$:5%Ce substantially matches the 3.1% already measured in 2006 with the same crystal and reported in [10] demonstrating good stability of its performance.

The spectra in Fig. 5 are calibrated using the 662 keV gamma ray of ^{137}Cs. The inset of Fig. 5 shows the low energy end of the spectra where the 32.06 keV X-ray from ^{137}Cs (Ba $K\alpha_{1,2}$ X-ray fluorescence) is detected. Each of the three spectrometers show a slightly different behavior: because of their actual nPR characteristic the 32.06 keV peak is detected at different energies – that is ~28.0 keV for $CeBr_3$, ~30.5 keV for $LaBr_3$:5%Ce and ~36.0 keV for NaI(Tl) – in good agreement with their respective nPR characteristics in Fig. 4 and [22]. Note that, in case of $LaBr_3$:5%Ce, the 32.06 keV peak is partially merged with that at 37.4 keV proper of ^{138}La electron capture decays (Ba K-shell binding energy) but detected at ~35.5 keV because of the nPR [26]).

The ^{152}Eu spectra in Fig. 6 shows how $CeBr_3$ still provides all the spectroscopic capability of $LaBr_3$:5%Ce with the only exception of the triple peak at 1085.9 keV+1089.7 keV+1112.1 keV, which is not very well resolved by $LaBr_3$:5%Ce neither. In particular in Fig. 6, the underneath intrinsic activity of $LaBr_3$:5%Ce may give the impression of a higher detection efficiency which is not the case.

More pulse height spectra were collected with the $2'' \times 2''$ $CeBr_3$ (SFB 308) using radioactive sources and in particular ^{228}Th and

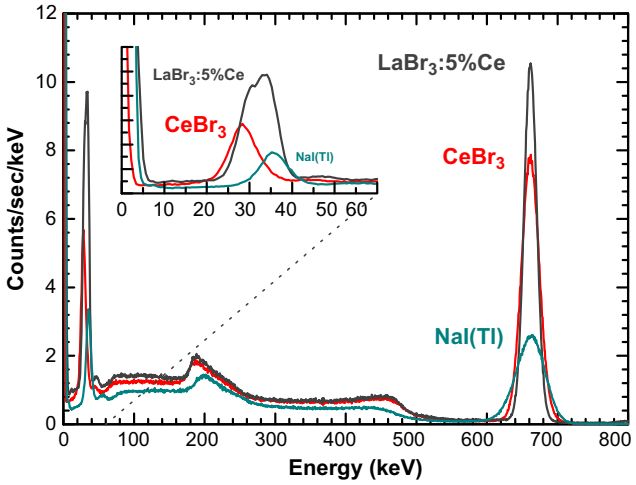

Fig. 5. Pulse height spectra of ^{137}Cs collected with $2'' \times 2''$ spectrometers based on $CeBr_3$, $LaBr_3$:5%Ce and NaI(Tl).

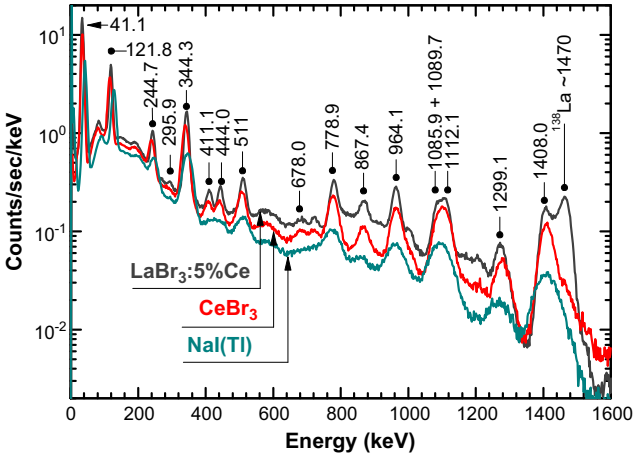

Fig. 6. Pulse height spectra of ^{152}Eu collected with $2'' \times 2''$ spectrometer based on $CeBr_3$, $LaBr_3$:5%Ce and NaI(Tl).

daughters for the highest energy gamma rays. Results in terms of FWHM vs. energy are plotted in Fig. 7 together with the equivalent results already obtained with the $2'' \times 2''$ $LaBr_3$:5%Ce taken from [10].

For both, $CeBr_3$ and $LaBr_3$:5%Ce, the first notable aspect is that the energy resolution can be fitted with a nearly exact function of $1/\sqrt{E}$, and in particular we found:

$$R(\%) = \begin{cases} 108 \cdot E^{-0.498} \sim 108/\sqrt{E} & for\ CeBr_3 \\ 81 \cdot E^{-0.501} \sim 81/\sqrt{E} & for\ LaBr_3 5\%Ce \end{cases} \quad (2)$$

where E is the gamma-ray energy. Typically this means that the energy resolution is dominated by statistical contributions and/or constant ones, or, as more likely in this case, that other present contributions scale as well as $1/\sqrt{E}$.

In order to investigate the results we can divide the energy resolution R (the one measured experimentally) into three main components as:

$$R^2 = R_{stat}^2 + R_{nPR}^2 + R_{inh}^2 \quad (3)$$

with R_{stat} the statistical contribution, R_{nPR} the nPR contribution and R_{inh} the contribution due to sample inhomogeneities as, inhomogeneous LY response across the crystal, inhomogeneous reflection at the surface etc.

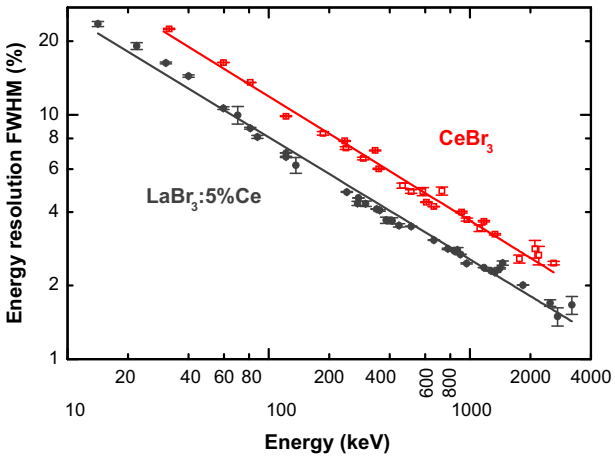

Fig. 7. Energy resolution FWHM as function of photon energy for $2'' \times 2''$ spectrometer based on $CeBr_3$ and $LaBr_3$:5%Ce. The lines are the best fitting function of Eq. (2).

In [10], it was argued for $LaBr_3$:5%Ce that most of the difference between the experimentally observed energy resolution R and R_{stat} originates from the poor variance of the electron multiplication in the PMT which must be operated for $LaBr_3$:5%Ce at half the manufacturer's recommended bias in order to avoid signal saturation. Recent results [27] demonstrate that the nPR strongly contributes to the actual limit of R, and hence that not all the worsening of the energy resolution (compared to the R_{stat}) can be attributed to a poor multiplication variance.

With the collected experimental data, we can evaluate R_{nPR} contribution to the overall energy resolution at 662 keV. From Table 1, the assessed photon-electron yield for large, $2'' \times 2''$ packed crystals of $CeBr_3$ and $LaBr_3$:5%Ce are 13,000 ph/MeV and 19,000 ph/MeV, respectively, and these values can be used for an evaluation of the R_{nPR} contributions. The photon–electron yield contributes to the statistical term of the spectrometer energy resolution as:

$$R_{stat} = 235\sqrt{\frac{1+\nu}{N_{ph}}} = \begin{cases} 73/\sqrt{E} & for\ CeBr_3 \\ 60/\sqrt{E} & for\ LaBr_3 5\%Ce \end{cases} \quad (4)$$

where: ν is the variance for the PMT electron multiplication (typically $1+\nu=1.25$) and N_{ph} is the photon-electron yield. With the energy E expressed in keV, N_{ph} is 13 phe/keV and 21 phe/keV for $CeBr_3$ and $LaBr_3$:5%Ce respectively. At the energy of 662 keV, Eq. (4) corresponds to 2.8% for $CeBr_3$ and to 2.3% for $LaBr_3$:5%Ce which compare to the measured R values of 4.1% and 3.2%, respectively.

Inhomogeneities are effective in worsening the energy resolution with the scaling up of the crystal size. For $CeBr_3$ and $LaBr_3$:5% Ce we have assessed that small bare crystal provide the best energy resolution, i.e., at 662 keV, 3.7% vs. 4.1% for $CeBr_3$ (see Table 1) and 2.7% vs. 3.2% for $LaBr_3$:5%Ce [27]. Assuming negligible the R_{inh} for small bare samples, using Eq. (3) we can calculate a R_{inh} contribution of about 1.0% for both, $CeBr_3$ and $LaBr_3$:5%Ce, large crystals.

We can then evaluate the R_{nPR} contribution at the energy of 662 keV as:

$$R_{nPR}(\%) \sim \sqrt{R^2 - R_{stat}^2 - R_{inh}^2} = \begin{cases} = 2.9\% & for\ CeBr_3 \\ = 1.8\% & for\ LaBr_3 5\%Ce \end{cases} \quad (5)$$

The above quantifies the impact of the nPR on the overall energy resolution. We therefore conclude that the larger R_{nPR} of $CeBr_3$ is consistent with the wider deviation of its nPR curve (Fig. 4).

For $LaBr_3$:5%Ce experimental results show that co-doped samples can indeed provide an energy resolution as good as 2.0% [27]

by "straightening" the nPR curve. Preliminary results already showed that the above technique apply to $CeBr_3$ as well and provided evidence that $CeBr_3$ with energy resolution as good as at least ~3% can be made by reducing its nPR.

5. Intrinsic activity

A low intrinsic activity is the asset of $CeBr_3$. Intrinsic activity was measured as background spectrum with the scintillator spectrometers placed inside a 15 cm thick lead castle in order to reduce the contributions of environmental radiation sources. The inner side of the lead castle included a copper coating to reduce the lead fluorescence X-rays. In addition, the measurements were performed using a PMT with low ^{40}K content (Electrontubes 9266B).

In order to evaluate the contribution of residual environmental activity (not shielded by or present in the lead castle) and of cosmic rays on the intrinsic activity measurements, the background spectrum of a $2'' \times 2''$ NaI(Tl) was also measured. NaI(Tl) is one of the cleanest scintillators in terms of intrinsic activity and it can provide an effective evaluation of the environmental activity inside the lead castle.

Intrinsic activity spectra of two samples of $CeBr_3$, one of $LaBr_3$:5%Ce and one of NaI(Tl), all $2'' \times 2''$ spectrometers, are shown in Fig. 8. Intrinsic activity spectra of five $1'' \times 1''$ samples of $CeBr_3$, later used for the radiation tolerance assessment, are shown in Fig. 9. All spectra are normalized by acquisition time, sample volume and keV per channel. The measurements lasted a minimum of 10 hours which corresponds to a minimum of $\sim 10^5$ collected counts for the $2'' \times 2''$ samples and of $\sim 10^4$ for the $1'' \times 1''$ samples. For all tested samples, the intrinsic activity expressed as specific integral count rate (counts/s/cm^3) in the energy range 20 keV–3 MeV is reported in Table 2. Data on a $1'' \times 1''$ $LaBr_3$:5%Ce sample are also included, taken from the measurements in [26] and revaluated for a consistent comparison. As measured with the $2'' \times 2''$ NaI(Tl) spectrometer, residual environmental activity and cosmic rays contribute to the specific integral count rate with ~0.01 counts/s/cm^3 (see Table 2).

Ce and Br elements do not present any naturally occurring radioactive isotope and $CeBr_3$ intrinsic activity is mainly due to radioactive impurities present in the raw materials. As seen in Figs. 8 and 9, some of our $CeBr_3$ samples show, in the energy range 1.2 MeV–2.2 MeV, an intrinsic activity due to alpha particle emitting impurities. Similar alpha contamination is always observed

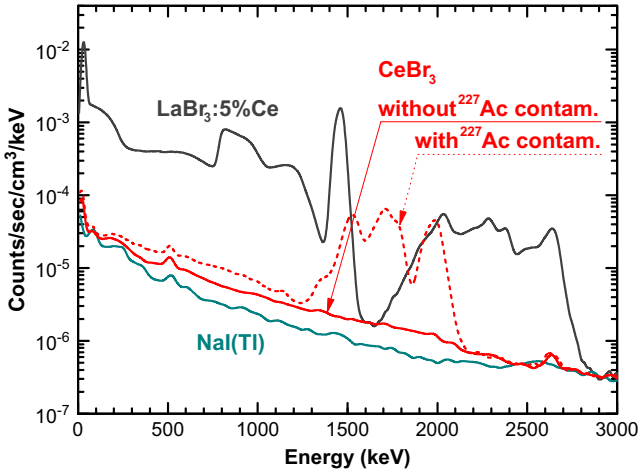

Fig. 8. Intrinsic activity spectrum of $CeBr_3$, $LaBr_3$:5%Ce and NaI(Tl) $2'' \times 2''$ spectrometers. For $CeBr_3$ two spectra are reported corresponding to crystal with and without ^{227}Ac contamination.

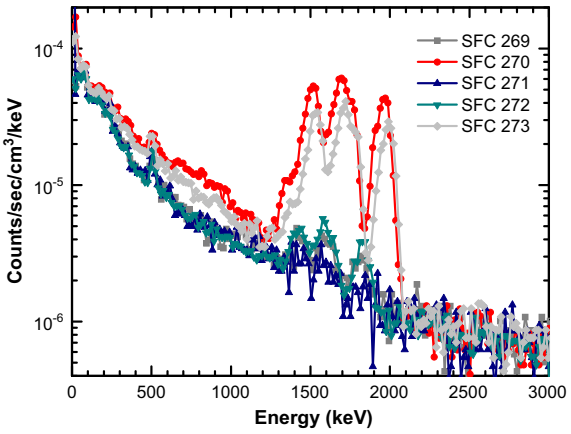

Fig. 9. Intrinsic activity spectrum of 5 $CeBr_3$ spectrometers with dimension of $1'' \times 1''$.

Table 2
Summary of the intrinsic activity measurements. Total activity is evaluated in the energy range 20 keV–3 MeV. Net ^{227}Ac activity is evaluated in the gamma-ray equivalent energy ranges of 1.2 MeV–2.2 MeV for $CeBr_3$ and 1.6 MeV–3 MeV for $LaBr_3$:5%Ce (see text). Measurement errors are due to uncertainties in the energy calibration for the total activity and to background subtraction for the net ^{227}Ac activity evaluation.

Material	Sample	Total activity counts/s/cm^3	Net ^{227}Ac activity counts/s/cm^3
$1'' \times 1''$ samples – 12.9 cm^3			
$CeBr_3$	SFC 269	0.023 ± 0.001	< 0.001
	SFC 270	0.051 ± 0.004	0.019 ± 0.001
	SFC 271	0.022 ± 0.001	< 0.001
	SFC 272	0.022 ± 0.002	0.001 ± 0.0005
	SFC 273	0.040 ± 0.001	0.011 ± 0.001
$LaBr_3$:5%Ce	sample in [26]	1.185 ± 0.006	0.019 ± 0.001
$2'' \times 2''$ samples – 102.9 cm^3			
NaI(Tl)	standard	0.012 ± 0.001	none
$CeBr_3$	SBX 431	0.019 ± 0.001	0.001 ± 0.0005
	SFB 308	0.043 ± 0.001	0.022 ± 0.001
$LaBr_3$:5%Ce	sample in [10]	1.242 ± 0.008	0.027 ± 0.001

for $LaCl_3$:10%Ce and $LaBr_3$:5%Ce and ascribed to ^{227}Ac and daughters with an evaluated ^{227}Ac concentration expressed in ^{227}Ac atoms per La atoms ranging from 10^{-13} to 10^{-15} [28,29]. The specific net activity of the ^{227}Ac alpha particle regions of our samples is also reported in Table 2. Based on these data and assuming a detection efficiency of 100% for the alpha particles, we roughly evaluated for our most contaminated $CeBr_3$ samples (~0.02 counts/s/cm^3) the concentration of ^{227}Ac atoms per Ce atoms to be of the order of $4\ 10^{-16}$. Such an exiguous presence of ^{227}Ac may originate from the fact that Ac, La and Ce are chemically homologous elements and extremely difficult to separate one from the other. Or, ^{227}Ac contamination may even originate from the presence in the ore of U, and in particular of ^{227}Ac-parent-nucleus ^{235}U, not sufficiently purified by the raw material processing. Assuming ^{235}U in isotopic concentration (i.e. 0.72%) and secular equilibrium with daughters, we evaluated that a residual concentration of natural U at 1–10 ppm in U atoms per Ce atoms would be compatible with the observed ^{227}Ac contamination of ~0.02 counts/s/cm^3 in terms of alpha particles. An average 5 ppm in U atoms per Ce atoms in $CeBr_3$ would give rise to an activity of ~0.2 counts/s/cm^3 due to ^{238}U alone, which, clearly, was not detected. Therefore, unless to consider complex cases in which the ^{235}U presence in $CeBr_3$ is not in natural isotopic concentration with U and/or the secular equilibrium does not applies, we must conclude

that ^{227}Ac is the direct responsible of the alpha contamination. For $LaCl_3$:10%Ce and based on different measurement techniques, similar conclusions were already reported by [28].

$CeBr_3$, $LaBr_3$:5%Ce and NaI(Tl) intrinsic activity spectra in Fig. 8 include gamma rays associated to ^{238}U series (e.g. 352 keV from ^{214}Pb) and to ^{232}Th series (e.g. 239 keV from ^{212}Pb). However, these gamma rays were detected with similar intensities by all the spectrometers ($\sim 2\times10^{-4}$ counts/s/cm^3 for ^{214}Pb and $\sim 5\times10^{-5}$ counts/s/cm^3 for ^{212}Pb), strongly indicating that the gamma-ray origin is environmental rather than intrinsic, discouraging further analysis. Nevertheless, for a $CeBr_3$ crystal with low ^{227}Ac contamination (i.e. $\sim$0.001 counts/s/cm^3) an accurate investigation of its radioactive impurities is available in [30]; which reports for ^{227}Ac a measured massic activity of 0.30 ± 0.02 Bq/kg (equivalent to $\sim$0.002 counts/s/cm^3) in reasonable agreement with our measurements.

$CeBr_3$ samples present two well distinct levels of ^{227}Ac contamination, i.e. $\sim$0.001 counts/s/cm^3 (almost absent) and $\sim$0.02 counts/s/cm^3 (same as $LaBr_3$:5%Ce) as specifically seen in Fig. 9 and Table 2 among the five $1''\times1''$ samples. Recent investigations on pilot crystal growths have associated the choice of raw material batches with the level of ^{227}Ac contamination found in the crystals and, from now on, the contamination can be kept under control by growing the crystals only from selected batches. However, long term availability of raw materials with low ^{227}Ac content cannot be guaranteed at the present time.

Comparing the spectra in Figs. 8 and 9 it is also seen as the shape of the $CeBr_3$ specific intrinsic activity is nearly independent from the crystal size. The same does not apply to $LaBr_3$:5%Ce for which the different attenuation lengths and escape probabilities of the ^{138}La decay products present an altered impact on the formation of the internal background for different crystal sizes [26].

The energy scales in the spectra in Figs. 8 and 9 are calibrated using gamma rays. When present, the alpha peaks of $CeBr_3$ are found at lower gamma-ray equivalent energy than that of $LaBr_3$:5%Ce. By calibrating the energy of the $CeBr_3$ alpha peaks using the energy of the $LaBr_3$:5%Ce alpha peaks (in Fig. 10 for the $2''\times2''$ samples), apart from the ^{208}Tl gamma ray in the $LaBr_3$:5%Ce spectrum, the particular shape and structure of the peaks appear very similar for both materials, further confirming a common ^{227}Ac origin (note that because of the different gamma-ray energy scales the underneath gamma-ray background is not the same for the two materials). In Fig. 10, the alpha/gamma LY ratio of $CeBr_3$ appears to be $\sim$1.33 times lower than that of $LaBr_3$:5%Ce. Since the alpha/gamma ratio of $LaBr_3$:5%Ce is 0.35 that of $CeBr_3$ amounts then to 0.26. The 1.33 times lower alpha/gamma ratio of $CeBr_3$ is consistent with its stronger nPR compared to $LaBr_3$:5%Ce in Fig. 4. The non perfect overlap of the peak positions observed in Fig. 10 is attributed to alpha nPR. In fact, as it happens for gamma rays, alpha particles may also present nPR as already observed in $LaCl_3$:10%Ce [31].

6. Effect of intrinsic activity on detection sensitivity

The ability of a gamma-ray spectrometer to detect low intensity sources depends on its energy resolution and detection efficiency, and on the presence of interfering background, which can be due to, either or both, spectrometer intrinsic activity and/or environmental activity (extrinsic activity). The energy resolution is a more important requirement compared to the other two. In fact, a lack in detection efficiency or a large intrinsic background can to some extent be compensated by using a larger spectrometer and/or a longer acquisition time, however no equivalently trivial solution exists to compensate a lack of energy resolution of a particular spectrometer.

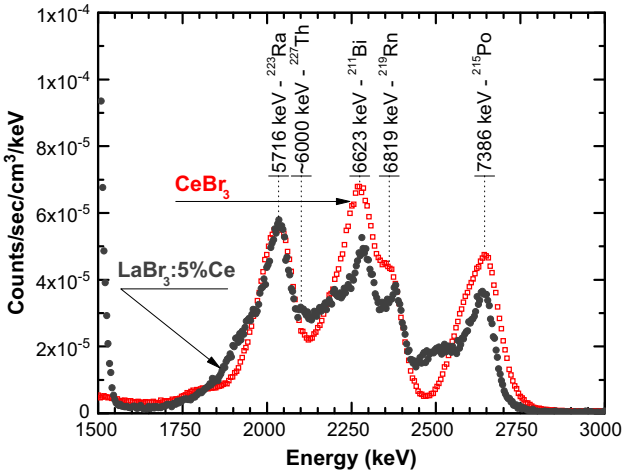

Fig. 10. $CeBr_3$ and $LaBr_3$:5%Ce intrinsic activity spectra of Fig. 8 ($2''\times2''$ samples) using a common energy calibration, i.e. that of $LaBr_3$:5%Ce. The 5 alpha peaks are labeled according to [28,31].

However, the beneficial effect of good energy resolution is often over stated. In fact, the ability to distinguish two peaks of nearly the same energy can take place only after that a significant detection of those peaks occurred. Moreover, not all applications require an extremely good energy resolution and, as we will see, moderately compromising in the energy resolution by choosing a $CeBr_3$ spectrometer instead of $LaBr_3$:5%Ce leads to a substantial advantage in the ability to detect low intensity emissions or, equivalently, to detect them faster.

In gamma-ray spectroscopy, the interfering presence of a background can be overcome by applying techniques of background subtraction. However, in some applications, the ability to perform measurements of background alone is limited or even not possible. This is the case, for instance, in planetary remote sensing, environmental monitoring and threat identification where the object under study itself is a source of background which will merge with the spectrometer intrinsic activity, making background subtraction techniques extremely difficult or even impossible.

Qualitatively, from Fig. 8 it can be seen as both $CeBr_3$ spectra, with or without ^{227}Ac contamination, clearly detect the 2614.5 keV gamma ray of ^{208}Tl (daughter of ^{232}Th), whereas this peak is not clearly observed with $LaBr_3$:5%Ce, because it overlaps with the alpha particle peaks. Neither is clearly observed with NaI(Tl) because of its lower detection efficiency and broader energy resolution. On the other hand, still in Fig. 8, in can be seen how the presence of ^{227}Ac contamination in $CeBr_3$ can interfere with the detection of ^{40}K.

By applying to our case the standard counting statistics, as, e.g., that described in [32], we can evaluate the impact of the intrinsic activity on the detection sensitivity as follows. A gamma-ray photopeak of energy E will be detected by a $2''\times2''$ $CeBr_3$ or $LaBr_3$:5%Ce spectrometer together with a number of intrinsic activity count $N_{bkg}(E,t)$ for which applies:

$$N_{bkg}(E,t)\propto f_{bkg}(E)\ R(E)\ t \tag{6}$$

where $f_{bkg}(E)$ and $R(E)$ are, respectively, the intrinsic activity and energy resolution at the energy E and t is the acquisition time. For $2''\times2''$ $CeBr_3$ and $LaBr_3$:5%Ce spectrometers we know experimentally $f_{bkg}(E)$ and $R(E)$ at all energies from 20 keV up to 3 MeV (see Fig. 8 and Fig. 7 respectively). Using the Gaussian distribution, we can then evaluate the standard deviation of $N_{bkg}(E,t)$ for every energy between 20 keV and 3 MeV as:

$$\sigma_{N_{bkg}}(E,t)=\sqrt{2\ f_{bkg}(E)\ R(E)\ t} \tag{7}$$

The ability of detecting a gamma ray depends on how many counts above σ_{Nbkg} it will produce in the acquired spectrum, which depends on source strength s, detection efficiency $\varepsilon(E)$ and acquisition time t. $CeBr_3$ and $LaBr_3$:5%Ce have almost equal Z_{eff} and density, so that the same $\varepsilon(E)$ can be used for both with little error introduced.

We can then formulate a figure of merit (FoM) which is proportional to the detection sensitivity for gamma rays as:

$$FoM(E,t)=\frac{s\ \varepsilon(E)\ t}{\sigma_{N_{bkg}}(E,t)}=s\ \varepsilon(E)\ \sqrt{\frac{t}{f_{bkg}(E)\ R(E)}} \tag{8}$$

with s the source strength in counts per second at the detector. Our FoM is in good agreement with the evaluation, in the context of gamma-ray astronomy, by Chupp [33] of the limiting gamma-ray flux that can be measured in presence of background.

To numerically evaluate the FoM we can use our experimentally measured energy resolution in Fig. 7 (but expressed in keV) and intrinsic activity in Fig. 8 (but expressed in counts/s/keV—being the volume of a $2''\times 2''$ crystal is 102.9 cm^3). For $\varepsilon(E)$ we can use the values published by [34] corresponding to the intrinsic detection efficiency of a $2''\times 2''$ $LaBr_3$:5%Ce (and $CeBr_3$) for a point source at the distance of ~15 cm from the spectrometer. We can then evaluate the FoM over the energy range 20 keV–3 MeV for $2''\times 2''$ spectrometers based on $LaBr_3$:5%Ce and on both cases of $CeBr_3$, i.e. with and without ^{227}Ac contamination. Results are plotted in Fig. 11 for a source of unity strength and for an acquisition time of 1 s.

The FoM in Fig. 11 applies when the intrinsic activity is the unique source of background. If other sources of background are present and known they can be included in $f_{bkg}(E)$. Multiplying the FoM by the number of standard deviations of the background fluctuations corresponding to a detectable signal (critical limit), the minimum detectable activity (MDA) can be evaluated, corresponding to the particular $f_{bkg}(E)$ and $\varepsilon(E)$ used.

From Fig. 11 and with respect to the most benign case of $CeBr_3$ without ^{227}Ac contamination, at the energy of 511 keV the values of the FoM are ~2 for $CeBr_3$ and ~0.4 for $LaBr_3$:5%Ce and, as consequence, to detect the 511 keV gamma ray to the same degree of confidence $LaBr_3$:5%Ce will need a time of $(2/0.4)^2=25$ times longer compared to $CeBr_3$. The lowest sensitivity of $LaBr_3$:5%Ce occurs around the ^{138}La intrinsic activity peak at 1471 keV [26],

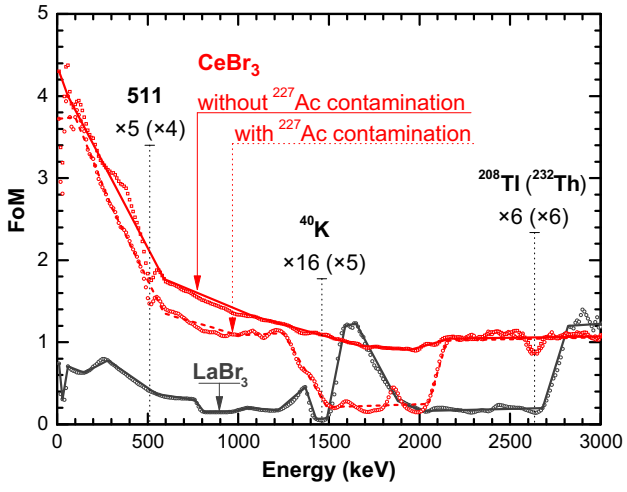

Fig. 11. $CeBr_3$ and $LaBr_3$:5%Ce detection sensitivity comparison. Two cases are shown for $CeBr_3$, with and without ^{227}Ac contamination. Original data points are plotted together interpolating lines to guide the eye. The reported multiplication factors at the gamma-ray lines of 511 keV, ^{40}K and ^{208}Tl(^{232}Th) correspond to the ratio of the FoMs of $CeBr_3$ and $LaBr_3$:5%Ce at that energies. Factors in brackets are for the $CeBr_3$ case with ^{227}Ac contamination.

where the ratio of the FoMs of $CeBr_3$ and $LaBr_3$:5%Ce is 16. This is well in agreement with the observation in [29] demonstrating $LaBr_3$:5%Ce strong lack of sensitivity for the detection of ^{40}K (1461 keV). At the ^{208}Tl(^{232}Th) gamma-ray line, the ratio of the FoMs of $CeBr_3$ and $LaBr_3$:5%Ce is ~6 whereas averaged over the energy range 20 keV–3 MeV, the ratio of the FoMs is ~5. Corresponding values for the $CeBr_3$ case with ^{227}Ac contamination are reported in brackets in Fig. 11. In this case, the average over the energy range 20 keV–3 MeV is ~4.

Apart from the limited, ~100 keV wide, energy range around 1.6 MeV, it is only above 2.8 MeV that $LaBr_3$:5%Ce sensitivity starts to exceed that of $CeBr_3$ because at those energies no intrinsic activity is present and because of $LaBr_3$:5%Ce better energy resolution, ~1.5% against ~2.0% of $CeBr_3$.

The FoM is evaluated using only the well characterized intrinsic activity. In real cases, what will determine the detection sensitivity is a combination of both the intrinsic and extrinsic activity. To evaluate this, we carried out an experiment in which a weak (~0.5 counts/s at the detector) 511 keV gamma-ray line from ^{22}Na source was detected by both $2''\times 2''$ $CeBr_3$ and $LaBr_3$:5%Ce spectrometers in the laboratory environment outside the lead castle. Energies slightly below 511 keV are relevant, e.g., for the detection of weapon grade plutonium (WGPu) [29]. Because of the laboratory environmental radiation and the Compton scattering of the 1274.6 keV gamma ray still from ^{22}Na, the background around the energy of 511 keV was ~10 times increased as compared to $CeBr_3$ intrinsic activity alone. Nevertheless, $CeBr_3$ still performed better than $LaBr_3$:5%Ce. In fact, applying the counting statistics in [32], for a 100 s acquisition time, $CeBr_3$ could detect the 511 keV gamma ray with 98% confidence whereas 85% confidence was achieved by $LaBr_3$:5%Ce which would instead need 400 s acquisition to provide the same 98% confidence as $CeBr_3$.

7. Proton activation

Using the AGOR superconducting cyclotron at the Kernfysisch Versneller Instituut (KVI), in Groningen, The Netherlands [35], we assessed the radiation tolerance of $CeBr_3$ scintillators for solar proton events (SPEs) in view of possible space applications. The experiment substantially repeated the one already performed for $LaBr_3$:5%Ce and reported in [36]. Again, 4 samples of dimension of $1''\times 1''$ (see Tables 1 and 2, sample SFC 272 was kept as reference), were irradiated with increasing proton fluences starting at 10^9 protons/cm^2 and then 10^{10}, 10^{11} and 10^{12} protons/cm^2 and with the proton energies replicating the slope of the August 1972 SPE energy spectrum [36].

Results show that, even for the highest fluence of 10^{12} protons/cm^2, which corresponds to over 1 Mrad Si-equivalent dose, $CeBr_3$ shows hardly any sign of degradation in energy resolution (Fig. 12) and/or light yield, making it an excellent candidate for space applications from the point of view of radiation tolerance.

Proton activation of $CeBr_3$ is substantially equivalent to that of $LaBr_3$:5%Ce and mainly due to the activation of Br, with production of instable ^{77}Kr and ^{79}Kr [37]. Activation of Ce is also observed with consequence production of ^{140}Cs, identified by the 602 keV gamma ray (see activation peak in Fig. 12). As for $LaBr_3$:5%Ce, $CeBr_3$ total activation decays with two main time constants a faster of ~20 h and a slower of ~1500 h. A more detailed report on the radiation tolerance assessment of $CeBr_3$ will be submitted as a separated publication.

8. Discussion and conclusions

Thanks to the advances in growing and detector–fabrication techniques, large $CeBr_3$ crystals and spectrometers are nowadays

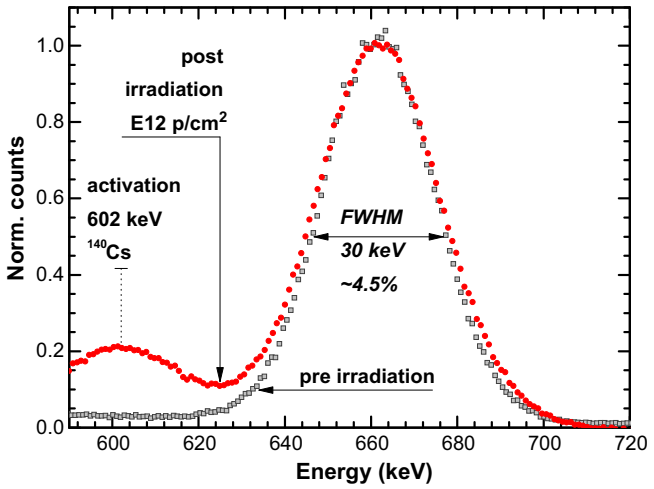

Fig. 12. Close-up of ^{137}Cs pulse height spectra collected with $CeBr_3$ $1'' \times 1''$sample SFC 273 (Tables 1 and 2) pre-irradiation and 16 days after irradiation with 10^{12} protons/cm^2.

available. Several $CeBr_3$ crystals up to $2'' \times 2''$ have been studied and compared to $LaBr_3$:5%Ce. $CeBr_3$ offers an energy resolution of ~4% at 662 keV mostly limited by the characteristic scintillation self-absorption and re-emission processes, which cause a lower LY compared to $LaBr_3$:5%Ce, and by its stronger nPR. At present we cannot provide data on $CeBr_3$ energy resolution above 3 MeV. At that energies, experience with $LaBr_3$:5%Ce [11,38] demonstrates that the energy resolution progressively worsens from a pure $1/\sqrt{E}$ dependence. If such behavior applies to $CeBr_3$ as well, this may tend to equalize $CeBr_3$ and $LaBr_3$:5%Ce energy resolutions above 3 MeV.

Below 3 MeV and thanks to its much reduced intrinsic activity, $CeBr_3$ detection sensitivity is, on average, about 5 times higher compared to $LaBr_3$:5%Ce and up to 16 times for the detection of ^{40}K. Some sample of $CeBr_3$ showed contamination due to ^{227}Ac, typical of $LaBr_3$:5%Ce, limiting to ~5 times higher its detection sensitivity for the ^{40}K. Nonetheless, recent investigations have identified the specific raw materials batches responsible for such a contamination and, through raw material screening, crystal growers are now able to produce $CeBr_3$ with none or very low ($\ll$0.02 counts/s/cm^3) ^{227}Ac contamination.

The results of the radiation tolerance assessment do not pose any concern for the space applications of $CeBr_3$ which can withstand protons fluence of 10^{12} protons/cm^2 ($>$ 1 Mrad Si-equivalent dose).

For applications such as remote gamma-ray spectroscopy of planetary surfaces, $CeBr_3$ ability to detect gamma ray with high sensitivity is an extremely important asset because of the low flux emissions expected from the planets. Furthermore, higher sensitivity leads to much faster acquisition times allowing to gain finer spatial resolution of the planet's gamma-ray map, with substantial benefit for the scientific goals. Similar benefits apply to other gamma-ray spectroscopy applications, as environmental radiation monitoring and homeland security, making of $CeBr_3$ an alternative to existing instruments.

Acknowledgments

Authors wish to thank Dr. R.W. Ostendorf and Dr. E.R. van der Graaf of the Kernfysisch Versneller Instituut, University of Groningen, for their support and assistance during the proton irradiations. The present work benefits from the European Space Agency (ESA) Contract no.: 4000103142/11/NL/AF.

References

[1] J. Masarik, R. Reedy, Journal of Geophysical Research 101 (1996) 18891.
[2] J. Brückner, J. Masarik, Planetary and Space Science 45 (1997) 39.
[3] I.G. Mitrofanov, et al., Planetary and Space Science 58 (2010) 116.
[4] G.F. Knoll, Radiation Detection and Measurement, 4th ed., John Wiley & Sons Inc., Hoboken, NJ, 2010.
[5] W. Drozdowski, et al., IEEE Transactions on Nuclear Science 55 (2008) 1391.
[6] SCHOTT AG – Advanced Materials, http://www.schott.com.
[7] Hellma Materials GmbH, http://www.hellma-materials.com.
[8] Scionix Holland B.V., http://www.scionix.nl.
[9] Saint-Gobain Crystals, http://www.detectors.saint-gobain.com.
[10] F. Quarati, et al., Nuclear Instruments and Methods in Physics Research Section A 574 (2007) 115.
[11] F.G.A. Quarati, et al., Nuclear Instruments and Methods in Physics Research Section A 629 (2011) 157.
[12] R.D. Shannon, Acta Crystallographica A32 (1976) 751.
[13] K.S. Shah, et al., IEEE Transactions on Nuclear Science 52 (2005) 3157.
[14] H.T. van Dam, et al., IEEE Transactions on Nuclear Science 59 (2012) 656.
[15] L.M. Bollinger, G.E. Thomas, Review of Scientific Instruments 32 (1961) 1044.
[16] G. Bizarri, et al., IEEE Transactions on Nuclear Science 53 (2006) 615.
[17] M. Bertolaccini et al., A technique for absolute measurement of the effective photoelectron per keV yield in scintillation counters, Presented at the Nuclear on Electronics Symposium, Versailles, France, September 1968.
[18] J.T.M. de Haas, P. Dorenbos, IEEE Transactions on Nuclear Science 55 (2008) 1086.
[19] P. Dorenbos, et al., IEEE Transactions on Nuclear Science 51 (2004) 1289.
[20] P. Dorenbos, et al., IEEE Transactions on Nuclear Science 42 (1995) 2190.
[21] Alan Owens, et al., Nuclear Instruments and Methods in Physics Research Section A 574 (2007) 158.
[22] I.V. Khodyuk, P. Dorenbos, IEEE Transactions on Nuclear Science 59 (2012) 3320.
[23] W.W. Moses, et al., IEEE Transactions on Nuclear Science 59 (2012) 2038.
[24] M. Moszyński, Radiation Measurements 45 (2010) 372.
[25] A. Kozorezov, et al., Journal of Applied Physics 112 (2012) 053709.
[26] F.G.A. Quarati, et al., Nuclear Instruments and Methods in Physics Research Section A 683 (2012) 46.
[27] M.S. Alekhin, et al., Applied Physics Letters 102 (2013) 161915.
[28] B.D. Milbrath, et al., Nuclear Instruments and Methods in Physics Research Section A 547 (2005) 504.
[29] B.D. Milbrath, et al., Nuclear Instruments and Methods in Physics Research Section A 572 (2007) 774.
[30] G. Lutter, et al., Nuclear Instruments and Methods in Physics Research Section A 703 (2013) 158.
[31] J.K. Hartwell, R.J. Gehrke, Applied Radiation and Isotopes 63 (2005) 223.
[32] G. Gilmore, Practical Gamma-ray Spectroscopy, second ed., Wiley & Sons Ltd, Chichester, UK, 2008.
[33] E.L. Chupp, Gamma-ray Astronomy (Nuclear Transition Region), D. Reidel Publishing Company, Dordrecht, Holland, 1976.
[34] M. Ciemala, et al., Nuclear Instruments and Methods in Physics Research Section A 608 (2009) 76.
[35] Kernfysisch Versneller Instituut (KVI), University of Groningen, www.rug.nl/kvi.
[36] Alan Owens, et al., Nuclear Instruments and Methods in Physics Research Section A 572 (2007) 785.
[37] E.-J. Buis, et al., Nuclear Instruments and Methods in Physics Research Section A 580 (2007) 902.
[38] A. Giaz et al., Nuclear Instruments and Methods in Physics Research Section A, http://dx.doi.org/10.1016/j.nima.2013.07.084, (in press).